Overcoming the compensatory elevation of NRF2 renders hepatocellular carcinoma cells more vulnerable to disulfiram/copper-induced ferroptosis

Xueying Ren [a,b,1], Yanchun Li [c,1], Yi Zhou [a,1], Wanye Hu [a], Chen Yang [d], Qiangan Jing [d], Chaoting Zhou [d], Xu Wang [e], Jiayu Hu [a], Luyang Wang [d], Jing Yang [a], Hairui Wang [a], Haifeng Xu [a], Huanjuan Li [a], Xiangmin Tong [a,d,f,***], Ying Wang [c,f,**], Jing Du [a,*]

[a] Laboratory Medicine Center, Department of Laboratory Medicine, Zhejiang Provincial People's Hospital, Affiliated People's Hospital, Hangzhou Medical College, Hangzhou, Zhejiang, 310014, China
[b] Department of Laboratory Medicine, The Second Affiliated Hospital of Zhejiang Chinese Medical University, Hangzhou, Zhejiang, 310005, China
[c] Department of Central Laboratory, Affiliated Hangzhou First People's Hospital, Zhejiang University School of Medicine, Hangzhou, Zhejiang, 310006, China
[d] Laboratory Medicine Center, Clinical Research Institute, Zhejiang Provincial People's Hospital, Affiliated People's Hospital, Hangzhou Medical College, Hangzhou, Zhejiang, 310014, China
[e] The Key Laboratory for Human Disease Gene Study of Sichuan Province, Prenatal Diagnosis Center, Sichuan Provincial People's Hospital, University of Electronic Science and Technology of China, Chengdu, Sichuan, 610072, China
[f] Phase I Clinical Research Center, Zhejiang Provincial People's Hospital, Affiliated People's Hospital, Hangzhou Medical College, Hangzhou, Zhejiang, 310014, China

ARTICLE INFO

ABSTRACT

Hepatocellular carcinoma (HCC) is one of the paramount causes of cancer-related death worldwide. Despite recent advances have been made in clinical treatments of HCC, the general prognosis of patients remains poor. Therefore, it is imperative to develop a less toxic and more effective therapeutic strategy. Currently, series of cellular, molecular, and pharmacological experimental approaches were utilized to address the unrecognized characteristics of disulfiram (DSF), pursuing the goal of repurposing DSF for cancer therapy. We found that DSF/Cu selectively exerted an efficient cytotoxic effect on HCC cell lines, and potently inhibited migration, invasion, and angiogenesis of HCC cells. Importantly, we confirmed that DSF/Cu could intensively impair mitochondrial homeostasis, increase free iron pool, enhance lipid peroxidation, and eventually result in ferroptotic cell death. Of note, a compensatory elevation of NRF2 accompanies the process of ferroptosis, and contributes to the resistance to DSF/Cu. Mechanically, we found that DSF/Cu dramatically activated the phosphorylation of p62, which facilitates competitive binding of Keap1, thus prolonging the half-life of NRF2. Notably, inhibition of NRF2 expression via RNA interference or pharmacological inhibitors significantly facilitated the accumulation of lipid peroxidation, and rendered HCC cells more sensitive to DSF/Cu induced ferroptosis. Conversely, fostering NRF2 expression was capable of ameliorating the cell death activated by DSF/Cu. Additionally, DSF/Cu could strengthen the cytotoxicity of sorafenib, and arrest tumor growth both *in vitro* and *in vivo*, by simultaneously inhibiting the signal pathway of NRF2 and MAPK kinase. In summary, these results provide experimental evidence that inhibition of the compensatory NRF2 elevation strengthens HCC cells more vulnerable to DSF/Cu induced ferroptosis, which facilitates the synergistic cytotoxicity of DSF/Cu and sorafenib.

* Corresponding author. Laboratory Medicine Center, Department of Laboratory Medicine, Zhejiang Provincial People's Hospital, Affiliated People's Hospital, Hangzhou Medical College, Hangzhou, 310014, China.
** Corresponding author. Phase I Clinical Research Center, Zhejiang Provincial People's Hospital, People's Hospital of Hangzhou Medical College, Hangzhou, Zhejiang, 310014, China.
*** Corresponding author. Phase I Clinical Research Center, Zhejiang Provincial People's Hospital, People's Hospital of Hangzhou Medical College, Hangzhou, Zhejiang, 310014, China.
E-mail addresses: tongxiangmin@163.com (X. Tong), nancywangying@163.com (Y. Wang), dujing1@hmc.edu.cn (J. Du).
[1] These authors contributed equally to this work.

1. Introduction

With the rapid growth of cancer incidence, liver cancer has been the sixth most diagnosed cancer worldwide. This trend is also observed in cancer mortality, makes HCC become the third leading cause of cancer-related death globally [1]. In particular, hepatocellular carcinoma (HCC) is the most common type of liver cancer, accounting for about 80% of all liver cancers. The main treatments for HCC include surgical excision, interventional therapy, and targeted drug therapy [2]. Despite significant achievements have been made in diagnosis and therapeutics, its clinical prognosis is still unsatisfactory. The majority of patients with liver cancer were diagnosed at an advanced stage or even with distant metastases, thus missing the opportunity for surgical resection. The five-year disease-free survival rate was approximately 18% [3], with a median survival time of 1 year. Therefore, it is imperative to develop more effective and less toxic therapies that sensitize cancer cells to chemotherapy agents.

Iron is an indispensable element that serves as catalysts and cofactors in living organisms, and takes part in various physiological processes. Generally, a certain amount of iron is crucial for cell survival, growth and proliferation, while too much labile Fe^{2+} is detrimental. As previously mentioned, amplifying cancer cells exhibit more dependence on iron than the non-malignant cells, which is termed iron addiction [4], revealing a prospect for cancer therapy through targeting the high level of free iron. Ferroptosis is a relatively new form of programmed cell death, which is initiated by iron-dependent lipid peroxidation [5,6]. Ferroptosis is sensitive and lethal to many tumor cells that are dependent on high labile iron. Thus, triggering ferroptosis in iron-rich tumors (such as HCC [7], PDAC [8], NSCLC [9] and breast cancer [10]) may provide insights into new therapeutic avenues or reverse drug-resistance in cancers.

Sorafenib [11], a FDA-approved first-line therapeutic drug, has been used to treat advanced HCC. However, the existence of drug resistance eventually leads to limited survival benefits [12]. Therefore, it's necessary to identify new molecular targets for HCC. Due to the high cost and long-time needed to develop a new therapeutic drug, drug-repurposing can be a faster and less costly alternative approach to the development of new drugs [13]. Disulfiram (DSF), an FDA-approved drug, has been used to treat alcoholism clinically for almost 70 years [14], with known pharmacokinetics and safety profiles. Recently, DSF has attracted attention as a potential anticancer drug, causing cancer cell death in a number of cancer types such as melanoma [15], glioblastoma [16], prostate cancer [17], and breast cancer [18]. It has been demonstrated that DSF could react with copper (Cu) to form an anti-cancer metabolite (DSF/Cu) and inhibit p97-dependent proteasome activity [19]. In HCC, some studies have found that DSF/Cu suppresses metastasis and induces cell death through NF-KB, TGF-β signaling and ROS-p38 MAPK pathway [20,21]. Although these findings indicate that DSF/Cu is capable of exerting anticancer effect in HCC, the underlying mechanism still needs to be further explored.

In this study, we identified that DSF/Cu selectively exhibited an efficient cytotoxic effect on hepatocellular carcinoma cell lines, and potently inhibited migration, invasion, and angiogenesis of HCC cells. Importantly, we found DSF/Cu could intensively impair mitochondrial homeostasis, increase free iron pool, enhance lipid peroxidation, and eventually resulting in ferroptotic cell death. Of note, a compensatory elevation of NRF2 accompanied the process of ferroptosis, which contributed to the resistance to DSF/Cu. Mechanistically, competitive interaction between p62 and Keap1 is responsible for the compensatory activation of NRF2. Both genetic or pharmacological inhibition of NRF2 rendered HCC cells more sensitive to DSF/Cu-induced ferroptosis. Moreover, DSF/Cu acted synergistically with sorafenib by simultaneously inhibiting the NRF2 and MAPK kinase signaling pathway and subsequently inducing ferroptosis. Additionally, DSF/Cu could intensively strengthen the cytotoxicity of sorafenib, and significantly reduce its effective concentration both *in vitro* and *in vivo*. In summary, these results provide experimental evidence that suppressing the compensatory elevation of NRF2 strengthens HCC cells more vulnerable to DSF/Cu induced ferroptosis, which facilitates the synergistic cytotoxicity of DSF/Cu and sorafenib.

2. Materials and methods

2.1. Chemicals, reagents, and antibodies

Assay kits for the detection of cell survival (CCK8 kit), GSH, ATP and MDA were purchased from Beyotime (Shanghai, China). Sorafenib, Ferrostatin-1 (Fer-1), Z-VAD-FMK, Necrosuifonamide (Necro), SB203580, SCH772984, SP600125 and ML385 were obtained from Selleck Chemicals (Houston, TX). DCF-DA MitoTracker, C11-BODIPY (581/591) and DAPI were obtained from Thermo Fisher Scientific (Waltham, MA). Rhodamine B-[(1,10- phenanthrolin-5-yl amino-carbonyl] benzyl ester (RPA) was obtained from Enzo Life Sciences (NY, USA). Deferoxamine (DFO), N-acetylcysteine (NAC), Cycloheximide (CHX), MG132, Disulfiram (DSF), $CuCl_2$ and Trigonelline hydrochloride were purchased from Sigma-Aldrich (St. Louis, MO, USA). The antibodies to NRF2 (ab62352), NQO1 (ab80588), P53 (ab179477), p21 (ab109520), p-p62 (ab211324), GAPDH (ab181602), γ-H2AX (ab81299), p62 (ab109012), MDA (ab6463) and β-actin (ab8226) were obtained from Abcam (Cambridge, MA). The antibody to 4-HNE (MAB3249) was obtained from Novus Biologicals (Littleton, CO, USA). The antibodies to p38 (9212S), p-p38 (9215S), ERK (4695S), p-ERK (4370S), JNK (9252s), p-JNK (9251s), HistoneH3 (3638), β-catenin (19807s), p-GSK3β (5558p), N-cadherin (4061p), Snail (3879p) and Vimentin (5741p) were purchased from Cell Signaling Technologies (Boston, MA, USA).

2.2. Cell culture

L02, Huh7, SMMC-7721 and 293T cells were preserved and passaged in our laboratory. These cells were grown in DMEM (Hyclone, Logan, UT, USA) with 10% fetal bovine serum (FBS) (Gibco, Grand Island, NY, USA), 100 U/ml penicillin and 0.1 mg/ml streptomycin (Beyotime, China). Cells were cultured in a humidified atmosphere of 5% CO_2 at 37 °C.

2.3. Cell viability assay

DSF and Cu were freshly mixed at a 1:1 ratio and used in this study. Cell viability was detected with CCK8 kit according to the manufacture's instruction. Cells were seeded on 96-well plates and treated with designed treatments, and then 10 μL CCK8 reagent was added to each well (containing 100 μL of medium), for further incubation at 37 °C for 1 h. Finally, the absorbance at 450 nm was measured by microplate reader. The cell viability in each group was calculated as the ratio to vehicle control.

2.4. Colony formation assays

Cells (3×10^3) were plated in plates and treated with the designed concentration of DSF/Cu for another 7 days. The colonies were fixed with 4% paraformaldehyde and stained with 0.1% crystal violet for 30 min. The stained colonies were photographed using an inverted microscope (Nikon, Tokyo, Japan) and colony numbers were counted with Image J software.

2.5. Transwell assay

HCC cells were seeded on the top of the transwell (Corning, USA) at a density of 4×10^4 cells per well in 200 μL serum-free medium. As a chemoattractant, 500 μL medium containing 10% FBS was placed in the lower chamber. After 24 h, the transwells were fixed with 4%

paraformaldehyde and stained with 0.1% crystal violet. Then, the cells on the top surface of the filter were removed using a cotton swab, and the cells migrated to the lower surface were observed and photographed using a light microscope (Nikon, Japan).

2.6. Wound-healing assay

SMMC-7721 cells (6.0×10^5) were added to 6-well plates and were grown to 80–90% confluence. A 10 μL sterile tip was used to create a linear scratch in the cell monolayer. The cells were washed and treated with different concentrations of DSF/Cu. The wound was imaged at 0, 24 h and 48 h. The relative migration rate was quantified using Image J software, and normalized to the control group.

2.7. Mitochondrial morphology

HCC cells (2×10^4) were seeded in confocal dish (35 mm with 20 mm bottom well, Cellvis, USA) and cultured overnight prior to treatment. The cells were treated with different concentrations of DSF/Cu for 6 h and then incubated with MitoTracker Red (100 nM) in a 37 °C incubator for 20 min. The living cells were visualized by laser confocal microscopy (Leica TCS SP5, German). Mitochondria were divided into three categories: the elongated tubular network mitochondria are classified as category I; large dotted mitochondria equally distributed all over the cytosol are classified as category II; totally fragmented mitochondria surrounding the nucleus are divided into category III.

2.8. Measurement of intracellular ROS accumulation

Intracellular superoxide accumulation was analyzed by the staining of fluorescent dye DCF-DA. After indicated treatments, cells were incubated with 4 μM DCF-DA in the dark for 30 min at 37 °C and then washed and suspended in DMEM. Intracellular ROS were determined by flow cytometry or microplate spectrophotometer (BioTek, USA), the fluorescent intensity represents the amount of cellular ROS generation.

2.9. Western blot

After treatments, cells were lysed in RIPA buffer with protease and phosphorylation inhibitor cocktail. Protein concentration was determined by BCA Protein Assay Kit (Thermo Fisher Scientific). Samples were separated by SDS-PAGE, and the proteins were then transferred onto PVDF membranes, followed by blocking with 5% milk-TBST, and incubated with the primary antibodies overnight. Membranes were then washed three times with TBST and incubated with horseradish peroxidase (HRP)-conjugated secondary antibodies. After washing three times with TBST, HRP was visualized using ECL Plus chemiluminescence detection kit (Thermo Fisher Scientific), and the signals were detected by Gel Imager (Bio-Rad).

2.10. Real-time quantitative polymerase chain reaction (RT-qPCR)

Total RNA was isolated by TRIzol (Life Technologies) according to the manufacturer's instructions, RNA was quantified by Nanodrop 1000 (Thermo Fisher). Reverse transcription was performed with Prime-Script™ RT reagent Kit (TAKARA, China) following the manufacture's protocol. Quantitative PCR was carried out using TransStart® Green qPCR SuperMix (TransGen Biotech, China) following the manufacture's recommendations. GAPDH and β-actin were served as the housekeeping gene. The primers for qPCR are indicated below: NRF2, forward, 5′-CACATCCAGTCAGAAACCAGTGG, reverse, 5′-GGAATGTCTGCGC-CAAAAGCTG; GAPDH, forward, 5′-GCACCGTCAAGGCTGAGAAC, reverse, 5′-ATGGTGGTGAAGACGCCAGT; β-actin, forward, 5′- CAC-CATTGGCAATGAGCGGTTC, reverse, 5′- AGGTCTTTGCGGATGTC-CACGT. The amplification efficiency varied between 90% and 105%. The relative expression level was calculated by $2^{-\Delta\Delta Ct}$ method.

2.11. Oxygen consumption rate (OCR) determination

Cells were seeded in XFe 24 seahorse cell culture microplate (Seahorse Bioscience) at a density of 3×10^4 cells/well. Meanwhile, the sensor cartridge was hydrated overnight at 37 °C. The next day, cells were treated with DSF/Cu using aforementioned concentrations for 6 h, plates were then incubated in a CO_2-free incubator at 37 °C for 1 h, OCR was measured real-time with sequential injection of 1.5 μM oligomycin, 1.5 μM carbonyl cyanide 4-(trifluoromethoxy) phenylhydrazone (FCCP) and 0.5 μM Antimycin A/Rotenone.

2.12. Co-immunoprecipitation

To detect the influence of DSF/Cu on the interaction between NRF2 and Keap1, cells transfected with exogenous Keap1 expression vector were treated with DSF/Cu for 12 h, then lysed with IP lysis buffer supplemented with protease and phosphorylation inhibitor cocktail for 60 min on ice, and centrifuged at 12,000 g for 10 min at 4 °C. The supernatants were incubated with Keap1 or Isotype IgG antibody overnight at 4 °C, following the co-incubation with protein A/G conjugated beads for 2 h at room temperature. Beads were washed with TBST three times, and then boiled in SDS-loading buffer and subjected to Western blot.

2.13. Animal experiments

BALB/c nude mice (aged 5 weeks) were purchased from Shanghai Laboratory Animal Center (Chinese Academy of Sciences) and kept in SPF condition for one week. Huh7 cells (2×10^6) were subcutaneously injected into the right flanks of BALB/c nude mice to establish tumors. Once the tumors reached approximately 100–200 mm^3, the animals were randomly divided into 4 groups. DSF/Cu-treated group was received oral administration of 50 mg/kg DSF and intramuscular injection of $CuCl_2$ (0.06 mg/kg) 2 h later. Sorafenib treated group was simultaneously received oral administration of 10 mg/kg sorafenib every day. For the combined therapeutic experiments, DSF, $CuCl_2$ and sorafenib were given to mice with an interval of 2 h. Tumor volumes and body weight were measured every 3 days during the course of the experiment.

2.14. Immunohistochemistry

Tumor xenograft tissues were fixed with 4% paraformaldehyde and embedded in paraffin. Then, the embedded tissues were cut into 4 μm sections and heated at 65 °C for 120 min, followed by de-paraffinized, hydrated and antigen retrieval. Endogenous peroxidases were blocked with 3% peroxide for 15 min, then sections were blocked in 5% BSA for 1 h and incubated overnight at 4 °C with primary antibodies. The primary antibodies used were anti-Ki67 (Abcam, ab15580, 1:100) and anti-NRF2 (Abcam, ab62352, 1:100). Biotinylated goat anti-rabbit IgG was used as secondary antibody and incubated at room temperature for 30 min. Then horseradish peroxidase-labeled streptavidin was added to the sections for 15 min at room temperature. DAB substrate was used to perform the chromogenic reaction. Images were acquired by the microscope (Nikon, Japan), and the expression levels of proteins were calculated by ImageJ software.

2.15. H&E analysis

Tumor xenograft tissues were fixed in 4% paraformaldehyde. The paraffin-embedded tissues were cut to 4 μm thickness and subjected to routine hematoxylin and eosin (H&E) staining according to the manufacture's instructions. Stained sections were viewed and photographed under a microscope (Nikon, Japan).

2.16. Statistical analysis

All statistical calculations were performed using GraphPad Prism (version 6.0). Data were presented as the mean ± standard deviation (SD) of three independent experiments. The differences between two groups were performed by the Student's *t*-test. Comparisons among multiple groups were analyzed by one-way ANOVA. $P < 0.05$ was considered to be significant.

3. Results

3.1. DSF/Cu inhibits cell viability, invasion and migration of HCC cells

To determine the cytotoxic effect of DSF/Cu on HCC cells, we firstly treated Huh7, SMMC-7721 and human fetal hepatocyte line L02 with different concentrations of DSF/Cu for 12 h and 24 h, and cell survival was assessed by CCK8 assay. Results showed that DSF/Cu exerts preferential toxicity towards HCC cells and selectively reduces its viability in a dose- and time-dependent manner, while sparing lower toxicity on the normal non-malignant cells (Fig. 1A). On the other side, mono treatment of DSF or Cu exhibited no obvious toxicity (Fig. S1A). Based on these observations, we next evaluated the long-term cell viability and colony formation capacity of HCC cells under the administration of DSF/Cu. Results indicated that a low concentration of DSF/Cu exerts pronounced long-term anti-neoplastic effects, and declines the formation of colonies with the increased DSF/Cu concentration (Fig. 1B). In addition, transwell and wound healing assays were performed to determine the effect of DSF/Cu on the invasion and migration of HCC cells. Results showed that DSF/Cu inhibits invasiveness of SMMC-7721 cells with a dramatic decline in the relative invasion rate (%), which is approximately 23% and 9% at the doses of 0.5 μM and 0.75 μM DSF/Cu (Fig. 1C). Consistently, DSF/Cu also effectively inhibits cell migration and weakens the EMT process, with the decreased expression of β-cadherin, N-cadherin, Vimentin and Snail (Figs. S1B and C). Collectively, these findings suggest that DSF/Cu restrains the cell viability, invasion and migration of HCC cells.
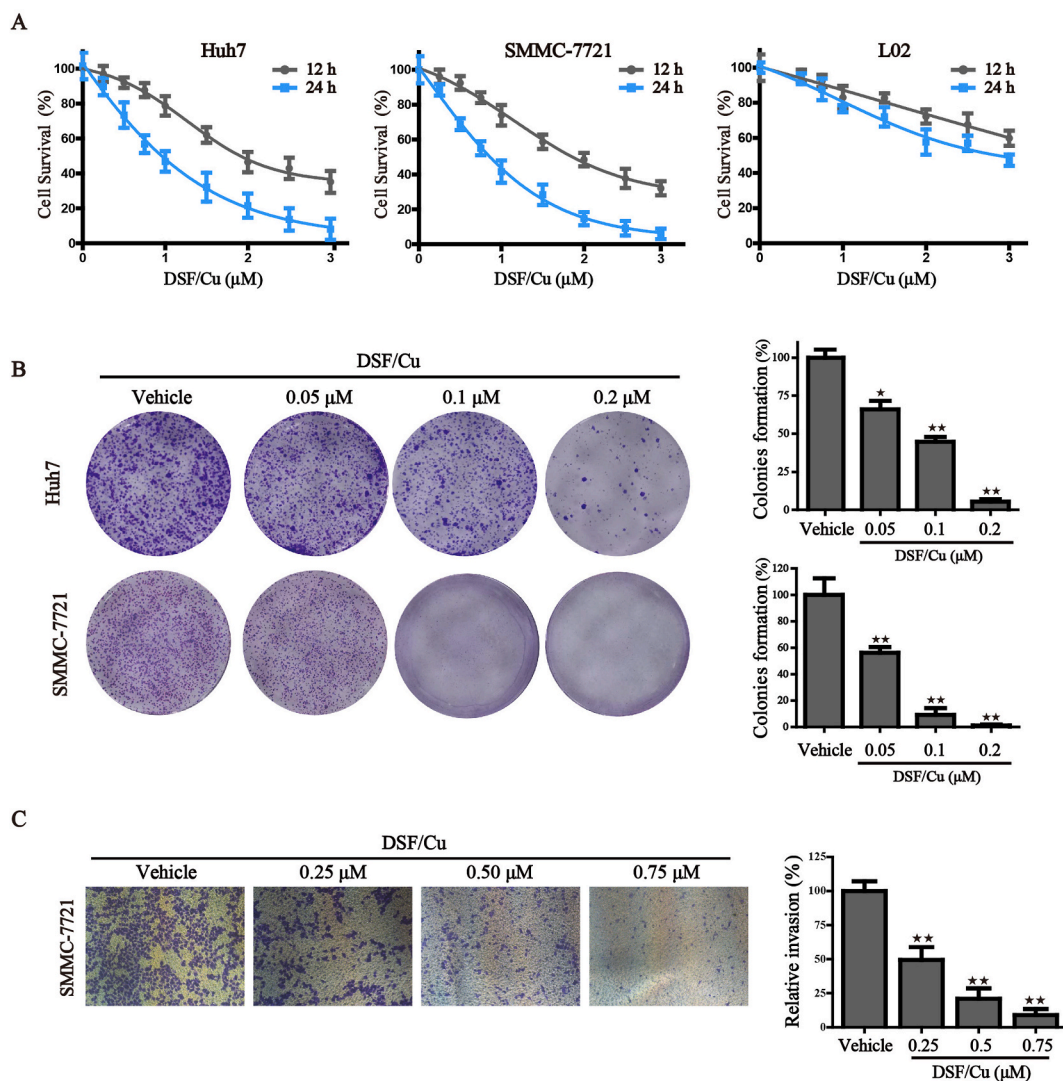

Fig. 1. DSF/Cu reduces the cell viability and proliferation in HCC cells.
(A) Human HCC cells Huh7, SMMC-7721 and normal hepatocyte L02 were treated with various concentrations of DSF/Cu (0–3.0 μM) for 12 h and 24 h. Cell viability was determined by CCK8 assay. (B) The colony formation of two HCC cells was performed under the treatment of DSF/Cu with different concentrations for 7 days. The colonies were photographed by inverted microscope; The corresponding quantitative histograms are shown on the right. (C) SMMC-7721 cells were treated with different concentrations of DSF/Cu for 24 h, and the cell invasion was detected by transwell assay. Corresponding quantitative histograms were shown on the right. Values represented mean ± SD. ★$P < 0.05$, ★★$P < 0.01$ versus control group.

3.2. DSF/Cu disrupts mitochondrial homeostasis and leads to oxidative disorder

Cellular proliferation, migration and metabolism heavily rely on the generation of sufficient ATP in mitochondria, the main organelle that coordinates a large fraction of metabolic, energetic, physiological processes, and ROS production [22]. We firstly focused on mitochondrial morphology, an intuitive feature of mitochondrial function, via labeling mitochondria with the MitoTracker Red probe. The results from confocal fluorescence microscope showed that an elongated-mitochondrial network appears in the control Huh7 and SMMC-7721 cells, while with exposure to increased concentrations of DSF/Cu, the mitochondria of HCC cells present to be fragmented and accumulating around the nucleus. Statistically, a pronounced increase of category II-III mitochondria was found under the increasing challenge of DSF/Cu, accompanied by the loss of healthy mitochondria (category I) (Fig. 2A). Once mitochondrial dysfunction occurs, mitochondrial oxidative phosphorylation process may be affected. We then explored the capacity of mitochondrial respiratory through Seahorse Xfe 24 Extracellular Flux Analyzer. The oxygen consumption rate (OCR) of basal respiratory, maximal respiratory, spare respiratory and ATP production were all significantly inhibited by the treatment of DSF/Cu (Figs. 2B and S2A). Additionally, DSF/Cu treatment significantly facilitated the accumulation of superoxide which may originate from the interrupted electron transport chain (Fig. 2C). Recent studies have indicated that DSF/Cu could induce antitumor activity via ROS-MAPK
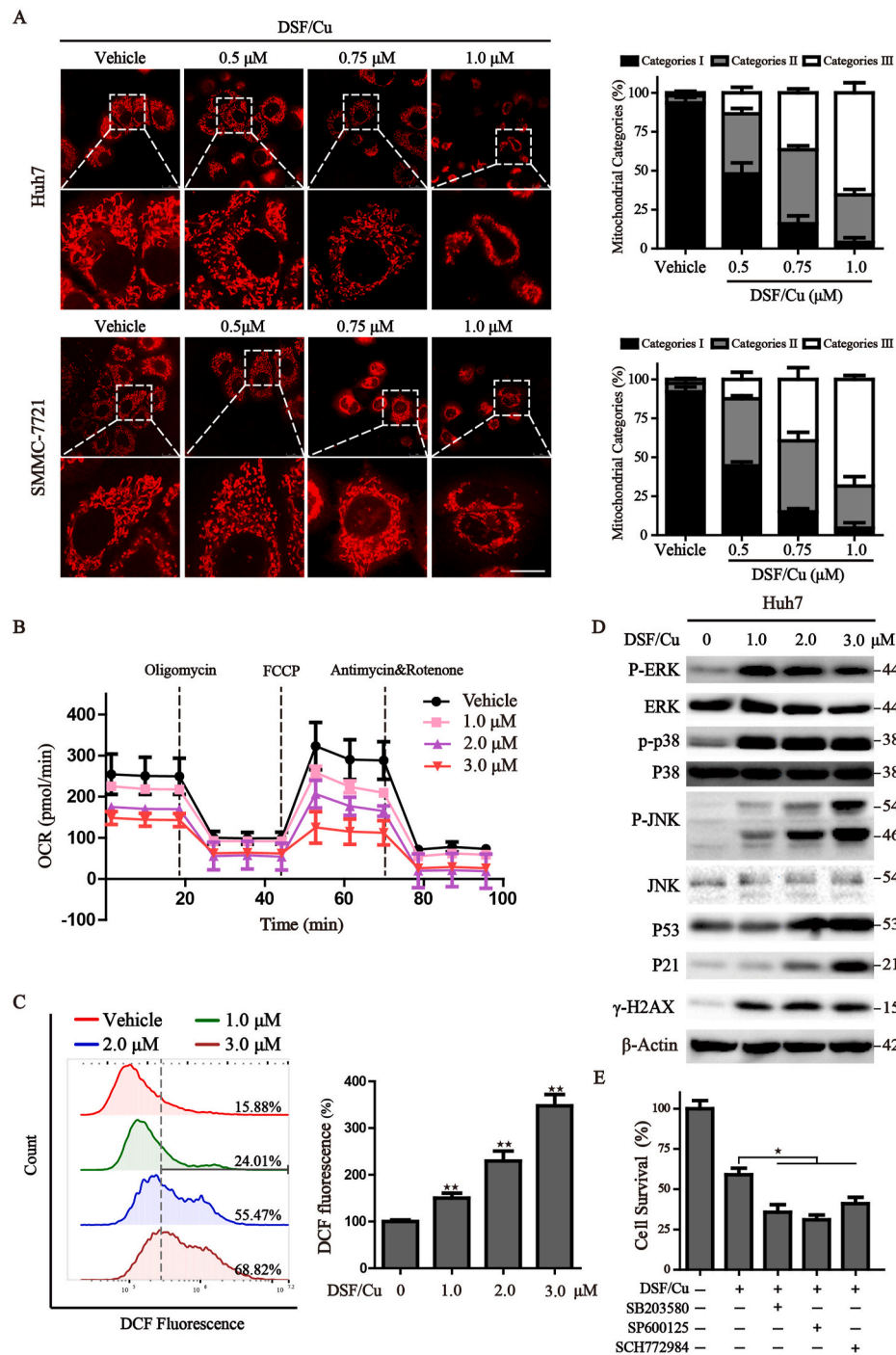

Fig. 2. DSF/Cu disrupts mitochondrial homeostasis and leads to oxidative disorder.
(A) After treatment with DSF/Cu for 6 h, the mitochondria in Huh7 and SMMC-7721 cells were visualized through MitoTracker red staining and observed by confocal microscopy. Scale bar: 5 μm. The statistical analysis of mitochondrial category was shown on the right. (B) Real-time analysis of OCR was carried out with Seahorse analyzer in DSF/Cu-treated HCC cells following the addition of oligomycin (1.5 μM), FCCP (1.5 μM) and antimycin A/Rotenone (0.5 μM). (C) Huh7 cells were treated with DSF/Cu for 8 h, intracellular superoxide was detected by DCF-DA staining and assayed by flow cytometry. The corresponding statistical histograms were shown on the right. (D) Western blot analysis of Huh7 cells after treatment with different concentrations of DSF/Cu for 12 h. β-actin was used as a loading control. (E) Cell viability analysis of Huh7 cells treated with DSF/Cu in the presence or absence of the indicated inhibitors was determined by CCK8 assay. Values represented mean ± SD. $\star P < 0.05$, $\star\star P < 0.01$ versus control.(For interpretation of the references to colour in this figure legend, the reader is referred to the Web version of this article.)

pathway [21,23]. We also discovered that the phosphorylated levels of p38, JNK and ERK, several components of the MAPK signaling pathway, were up-regulated after treatment of DSF/Cu (Figs. 2D and S2B). However, the inhibitors of P38 (SB203580), ERK (SCH772984) and JNK (SP600125) couldn't rescue the cytotoxic effect of DSF/Cu on HCC cells, demonstrating that MAPK activation is not the key event involved in the mechanism of DSF/Cu-induced cell death in HCC cells (Fig. 2E). To better characterize DSF/Cu-related events, we evaluated the presence of DNA oxidative damage and found that HCC cells displayed a significantly higher level of γ-H2AX, p53 and p21, indicating the appearance of DNA double-strand breaks (Fig. 2D). Overall, these findings confirm DSF/Cu could disrupt mitochondrial homeostasis and lead to oxidative stress.

3.3. DSF/Cu induces ferroptosis and simultaneously increases cellular NRF2 levels

To further characterize the basis of cell death induced by DSF/Cu, Huh7 cells were treated with DSF/Cu in the absence or presence of several cell death inhibitors. Results showed that DFO (iron chelator), ferrostatin-1 (ferroptosis inhibitor), GSH and NAC (antioxidant)

significantly alleviate cell viability impaired by DSF/Cu incubation, while Z-VAD-FMK (apoptosis inhibitor) and necrosulfonamide (necroptosis inhibitor) display slight recovery on the DSF/Cu-induced cell death (Fig. 3A). These findings indicate that ferroptosis might contribute to the main cytotoxic effect mediated by DSF/Cu. As the accumulation of free iron and the generation of lipid peroxides are two major hallmarks of ferroptosis. We first tested the formation of lipid peroxides by BODIPY staining and immunofluorescence staining of MDA and 4-HNE, two main secondary products of lipid peroxidation. Results from confocal microscopy showed that application of DSF/Cu increases the fluorescence of BODIPY, accelerates the staining of MDA and 4-HNE (Fig. 3B and C). To verify whether the increase of lipid peroxidation is due to the altered free iron pool. We examined the changes of iron metabolism by the following assays: (i) DSF/Cu induced free iron accumulation reflected by the decreased fluorescence of RPA, (ii) DFO administration ameliorates free iron accumulation and cellular lipid ROS peroxidation (Figs. 3C and S3A). Collectively, DSF/Cu promotes ferroptotic cell death by accelerating free iron accumulation and lipid peroxidation.

The nuclear factor erythroid 2-related factor 2 (NRF2), a key transcription factor, is responsible for the regulation of antioxidant response and plays a critical role in mitigating ferroptosis. We next analyzed the
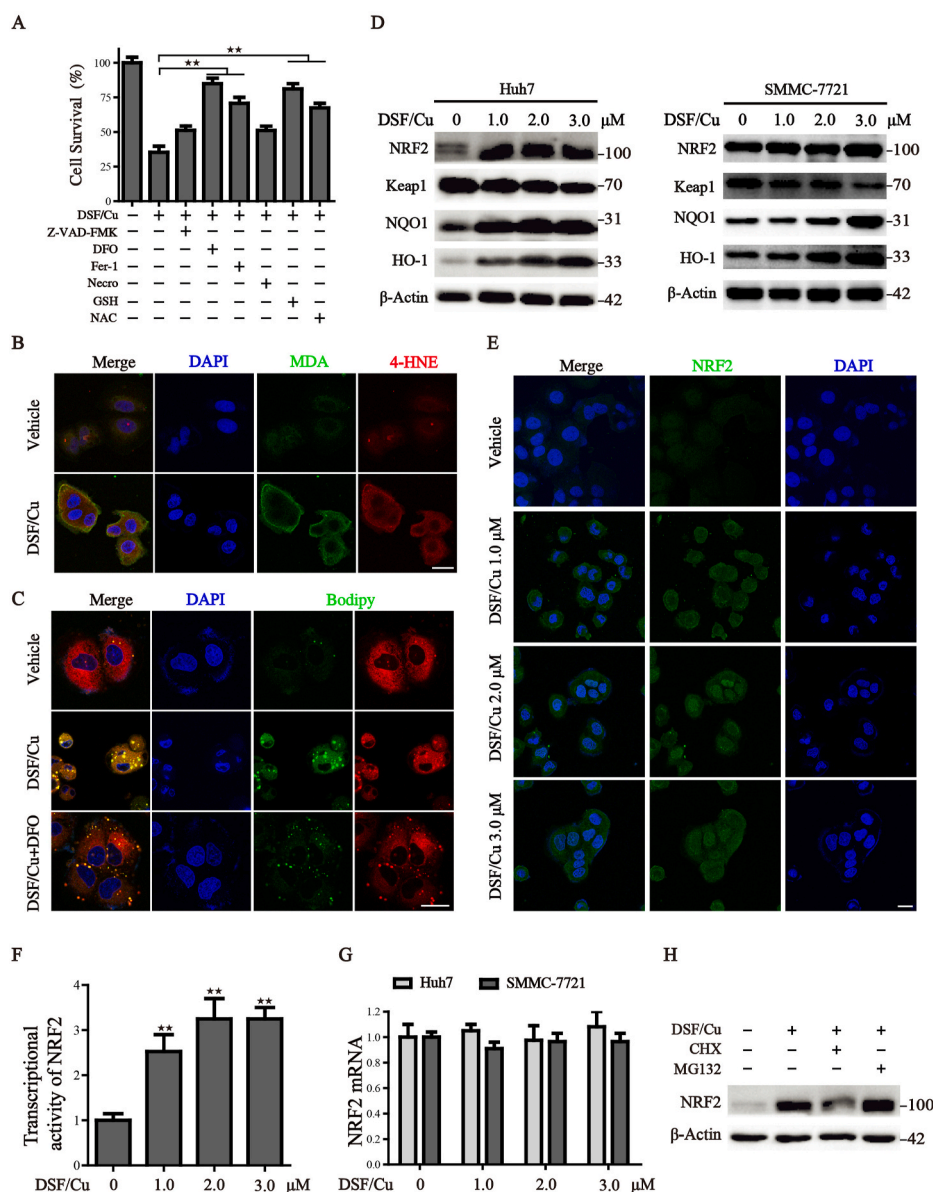

Fig. 3. DSF/Cu induces ferroptosis and simultaneously increases cellular NRF2 levels.
(A) Viabilities of Huh7 cells cultured with DSF/Cu in the presence or absence of various cell death inhibitors for 12 h. (B) Huh7 cells were treated with DSF/Cu (2 μM) for 8 h, immunofluorescence staining of MDA and 4-HNE were captured by confocal laser microscope. DAPI was used for nuclear staining. Scale bar: 10 μm. (C) Huh7 cells were cultured with DSF/Cu (2 μM) in the presence or absence of DFO (100 μM) for 8 h, confocal microscopy was used to monitor intracellular total lipid peroxides with lipophilic dye Bodipy. Scale bar, 10 μm. (D) Protein levels of NRF2, Keap1, NQO1 and HO-1 were assayed by Western blot in Huh7 and SMMC-7721 cells under the exposure of DSF/Cu for 12 h. (E) Representative images of NRF2 immunostaining in Huh7 cells treated with various concentrations of DSF/Cu for 12 h. Scale bar, 10 μm. (F) The transcriptional activities of NRF2 were assessed using the NRF2-responsive luciferase reporter assay system and normalized to the control cells. (G) Relative quantitative PCR was used to measure NRF2 mRNA expression, NRF2 mRNA is normalized to GAPDH. (H) Huh7 cells were treated with DSF/Cu alone or in combination with CHX or MG132 for 12 h. The protein level of NRF2 was assessed by Western blot. β-actin was used as a loading control. Values represented mean ± SD. ⋆P < 0.05, ⋆⋆P < 0.01 versus control.

expression and function of the NRF2 axis. Remarkably, treatment with DSF/Cu dramatically increased NRF2 protein expression, nuclear translocation, and transcriptional activity of NRF2, with subsequently upregulated the expression of NRF2 downstream proteins, including NQO-1 and HO-1 (Fig. 3D–F, S3B). But the mRNA of NRF2 was unchanged (Fig. 3G and S3C). This indicates that DSF/Cu-challenged NRF2 expression occurs in a transcription-independent manner. Therefore, cycloheximide (CHX, a chemical protein synthesis inhibitor) and MG-132 (a selective 26S proteasome inhibitor) were utilized to evaluate the stability of NRF2 protein under the challenge of DSF/Cu. The results from Western blot showed that CHX limited, whereas MG-132 augmented the compensatory elevation of NRF2 protein level (Fig. 3H), demonstrating that a post-transcriptional mechanism involves the regulation of NRF2 protein during DSF/Cu-mediated ferroptosis. Collectively, these data suggest that DSF/Cu could induce ferroptotic cell death, associated with a compensatory elevation of NRF2, which

may lower the sensitivity of DSF/Cu.

3.4. Inhibition of NRF2 enhances the sensitivity of HCC cells to DSF/Cu induced ferroptosis

To further explore whether the compensatory increased NRF2 expression modulates the anticancer activity of DSF/Cu, potent NRF2 inhibitors trigonelline (Trig) [24] and ML385 [25] were selected to uncover this issue. Indeed, inhibition of NRF2 by Trig or ML385 led to a remarkable synergistic inhibitory effect with DSF/Cu in a concentration-dependent manner (Fig. 4A, C). In addition, both of them could improve the response of HCC cells to DSF/Cu-induced oxidative stress (Fig. 4B, D). The colony formation assay also confirmed that suppression of NRF2 significantly accelerates the inhibitory effect on long-time survival following the treatment of DSF/Cu (Fig. 4E). We further isolated the cytoplasmic and nuclear proteins of treated cells and
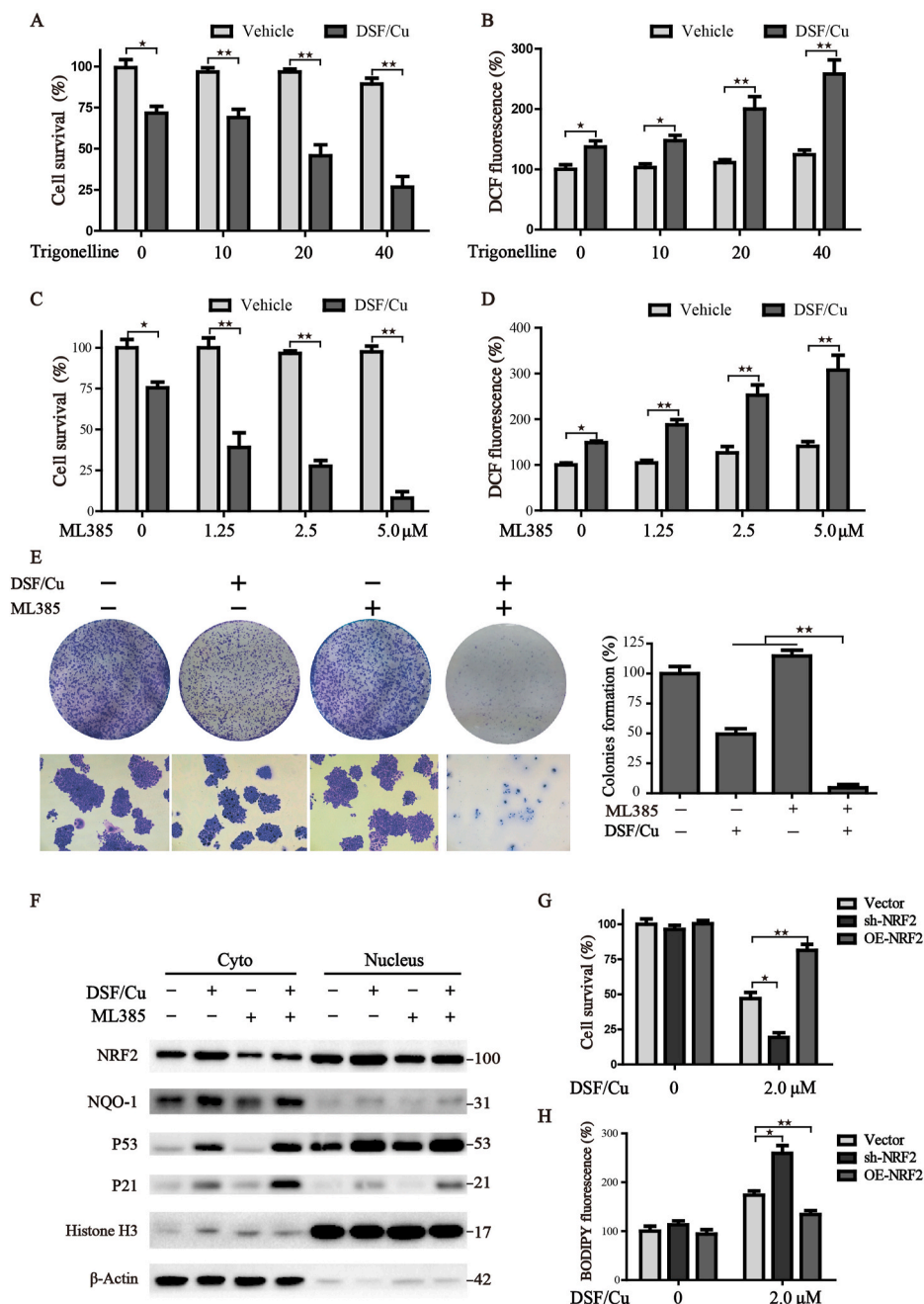

Fig. 4. Inhibition of NRF2 enhances the sensitivity of HCC cells to DSF/Cu-induced ferroptosis.

(A, C) Huh7 cells were treated with DSF/Cu (1 μM) alone or in combination with various concentrations of Trigonelline or ML385 for 12 h, and cell survival was assessed by CCK8. (B, D) Huh7 cells with indicated treatment were subjected to the DCF-DA staining to monitor the intracellular ROS, and the intensity of DCF fluorescence was determined by microplate spectrophotometer. (E) The colony-formation assay was performed under the treatment of DSF/Cu (0.1 μM) and/or ML385 (2.5 μM) for 7 days. The statistical histograms were shown on the right. (F) Cytoplasmic and nuclear proteins of treated cells were isolated and determined by Western blot. Cells with different expressions of NRF2 were treated with DSF/Cu. The cell survival (G) and lipid peroxides (H) were determined by CCK8 assay and BODIPY staining, respectively. All histograms were presented as mean ± SD, $*P < 0.05$, $**P < 0.01$ versus control.

verified the expression of NRF2 and its downstream targets by Western blot. Results showed that DSF/Cu facilitates the nuclear translocation of NRF2, and activates the downstream transcriptional expression of NQO-1, while application of ML385 could alleviate this phenomenon (Fig. 4F). Concomitantly, NRF2 inhibition exacerbated DSF/Cu-induced upregulation of p53 and p21. To further confirm the pharmacological data, stable NRF2 knockdown cells were generated through shRNA mediated lentivirus transfection. Consistent with the findings above, NRF2 silencing increased DSF/Cu-induced cell death and strengthened lipid peroxidation in HCC cells. Conversely, ectopic expression of NRF2 mitigated DSF/Cu-induced cytotoxicity (Fig. 4G–H, S3D). Altogether, these data demonstrate that either pharmacological or genetic inhibited the compensatory increased NRF2 could strengthen the DSF/Cu induced ferroptosis in HCC cells.

3.5. Competitive interaction between p62 and Keap1 is responsible for the compensatory activation of NRF2

We next focused on how the compensatory mechanism was activated to weaken the sensitivity of DSF/Cu-induced ferroptotic cell death. To address this issue, we evaluated the half-life of NRF2 protein under the pre-treatment of protein synthase inhibitor cycloheximide. Results demonstrated that DSF/Cu treatment prolongs the half-life of NRF2, suggesting the degradation of NRF2 is suppressed by DSF/Cu (Fig. 5A). Keap1 is the major upstream regulator of NRF2, and controls both the subcellular localization and steady-state levels of NRF2 [26]. It is identified that Keap1 binds the N-terminal Neh2 domain of NRF2 to promote its ubiquitination and subsequent degradation [27]. Therefore, we performed immunoprecipitation experiments to test the association between NRF2 and Keap1. Results illustrated that DSF/Cu dramatically dampens the interaction between NRF2 and Keap1 (Fig. 5B).
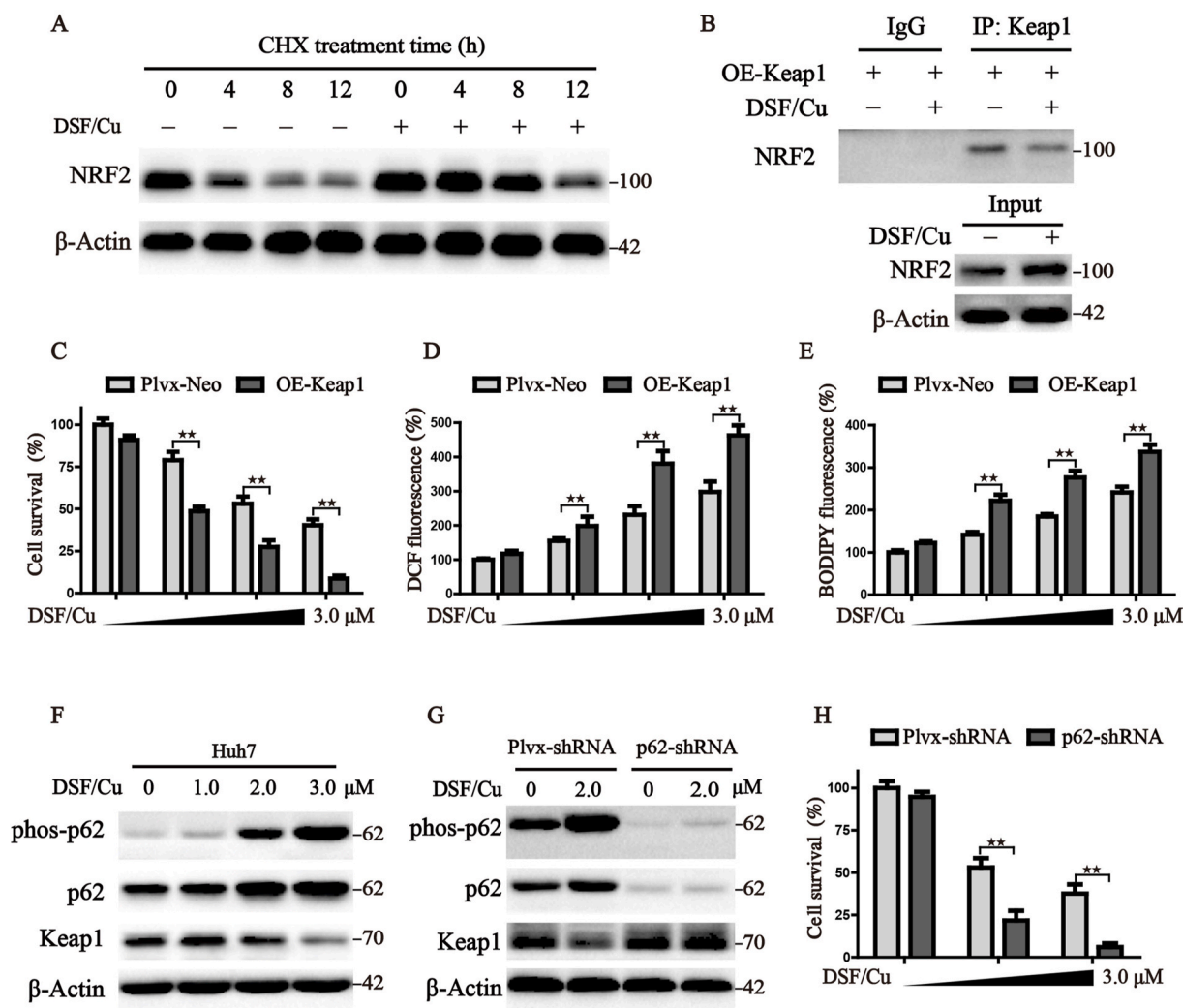

Fig. 5. Competitive interaction between p62 and Keap1 is responsible for the compensatory activation of NRF2.
(A) The half-life of NRF2 was analyzed in SMMC-7721 cells treated with or without DSF/Cu in the presence or absence of CHX (1 mg/ml) for different times. (B) Cells were treated with DSF/Cu for 12 h, the interaction between Keap1 and NRF2 was detected by Western blot. Huh7 cells transfected with Keap1 or control empty vector were treated with different concentrations (0–3.0 μM) of DSF/Cu; (C) Cell survival was detected by CCK8 assay; (D) ROS levels were measured by DCF-DA staining; (E) Lipid peroxides were detected by BODIPY staining. (F) Huh7 cells were exposed to different concentrations of DSF/Cu for 12 h, protein levels of p-p62, p62 and Keap1 were evaluated by Western blot. (G) Cells transfected with p62-shRNA or control vector were exposed to DSF/Cu (2.0 μM) for 12 h, the protein levels were detected by Western blot. (H) Control and p62 knockdown cells were treated with gradient of DSF/Cu for 12 h, cell survival was detected by CCK8 assay. All histograms were presented as mean ± SD ★$P < 0.05$, ★★$P < 0.01$ between indicated groups.

Furthermore, we enforced the expression of Keap1 through lentivirus transduction in HCC cells, and found that Keap1 overexpression sensitizes DSF/Cu-induced ferroptosis (Fig. 5C), together with increased ferroptotic events including accelerated superoxide production (Fig. 5D) and lipid peroxidation (Fig. 5E). Recently, researchers have confirmed that the substrate adaptor p62 modulates NRF2 expression by directly binding with Keap1 [7]. Indeed, p62 was upregulated with increased competitive binding Keap1 in response to DSF/Cu. In addition, increased phosphorylation of p62 was identified under the treatment of DSF/Cu (Fig. 5F), which markedly increased its binding affinity for Keap1, as demonstrated previously [28]. Moreover, knockdown of p62 reversed the loss of Keap1 (Fig. 5G), and facilitated the ferroptosis in the condition of DSF/Cu treatment (Fig. 5H). Overall, these findings reveal that the competitive binding ability of p62 to Keap1 is responsible for the compensatory activation of NRF2, rendering HCC cells more resistant to DSF/Cu-induced ferroptosis.

3.6. DSF/Cu acts synergistically with sorafenib against HCC tumors through induction of ferroptosis

Sorafenib is a first-line drug for advanced HCC, however, the development of drug resistance limits its efficacy. Our recent study illustrated that depletion of cysteine acts synergistically with sorafenib and renders HCC cells vulnerable to ferroptosis [29]. We further explored whether DSF/Cu acts synergistically with sorafenib through induction of ferroptosis, and verified this issue by the following assays: (i) DSF/Cu exacerbates sorafenib-induced ferroptosis in a dose-dependent manner, accompanied by increased ferroptotic events including accelerated superoxide production and lipid peroxidation (Fig. 6A–C). (ii) Combination of DSF/Cu and sorafenib exerts a high capacity in abrogating colony-forming (Fig. 6D). (iii) Similarly, DSF/Cu and sorafenib cooperatively abolished the invasion of HCC cells (Fig. 6E). We next evaluated the potential basis of the exhibited synergistic cytotoxicity. Considerable evidence has indicated that the activation of the Ras/MAPK signaling regulates not only cell growth, development and differentiation, but also hepatic carcinogenesis [30]. Sorafenib is a multi-kinase inhibitor that effectively inhibits the activation of MAPKs, and successfully targets HCC. Western blot analysis was performed to verify the activation of MAPK pathways. Results showed that sorafenib effectively eliminates the phosphorylation of p38, ERK, JNK which were activated by DSF/Cu treatment (Fig. 6F). The fractions of cytoplasm and nucleus were further isolated for immunoblotting, which manifested that sorafenib attenuates the nuclear translocation of NRF2 upon the treatment of DSF/Cu, as effectively as ML385. In addition, sorafenib concomitantly suppresses the downstream transcriptional expression of NQO-1, and aggravates the nuclear translocation of p53 (Fig. 6G). Overall, simultaneously inhibiting the NRF2 and MAPK kinase signaling pathway probably involves in the synergistic lethal effects of sorafenib and DSF/Cu.

3.7. Combination treatment of DSF/Cu and sorafenib effectively arrests tumor growth in vivo

We wondered whether the synergistic lethal effects of DSF/Cu and sorafenib exhibit therapeutic potential in the xenograft tumor. The subcutaneous tumor models bearing Huh7 cells were established, and randomly divided into four groups with indicated treatments. The weight of tumor-bearing mice was recorded as an indicator of drug toxicity. As shown in Fig. 7A, The group with DSF/Cu or/and sorafenib treatment didn't exert obvious weight loss, indicating the high security for clinical use. Consistent with *in vitro* data, the *in vivo* experiments further demonstrated that administration of DSF/Cu or sorafenib suppresses tumor growth, and the antitumor efficacy is more pronounced in the combination group (Fig. 7B). In addition, the immunohistochemical assay displayed that sorafenib acts synergistically with DSF/Cu to increase the area of necrosis, decrease the ki67 staining, and attenuates

the compensatory elevation of NRF2 (Fig. 6C). Moreover, exhausted GSH levels, diminished ATP production, and excess lipid peroxides accumulation were more pronounced in the combination treated group (Fig. 7D–F). Our findings show that the combination of sorafenib with DSF/Cu is not only tolerable but also beneficial, which may act as a promising therapy for treating hepatocellular carcinoma.

4. Discussion

Distinct lethal regimens are designed to selectively target cancer cells via different regulated cell death (RCD) processes, including ferroptosis, apoptosis, necroptosis, autophagic cell death and pyroptosis, etc. Each RCD process occurs through individual subroutines, and could be modulated by unique signal transduction pathways. It can also produce distinct morphological changes, and hence differentially affect tumor response to treatment. Usually, apoptosis is the most widely studied RCD to eliminate cancer cells. However, the clinical application of the therapeutic approach through activating apoptosis in oncology remains an insurmountable challenge for the high primary and acquired drug resistance rate [31]. Thus, the development of novel drugs for selectively targeting other forms of RCD may hold great promise for suppressing tumor growth.

Ferroptosis is a relatively new form of programmed cell death, which was first observed in cancer and defined in 2012 by Dixon [6]. The initiation of ferroptosis requires unrestricted lipid peroxidation in an iron-dependent manner, which is different from apoptosis, necroptosis and autophagy. Several signal transduction pathways including iron metabolism, GSH-GPX4, iron sulfur cluster assembly, mitochondrial energy metabolism and FSP1-COQ10 constitute the core molecular mechanism of ferroptosis [32–35]. Small molecule erastin was first discovered for specifically inducing ferroptosis in RAS mutant tumor cells, while sparing litter cytotoxicity to the non-malignant normal cells. Subsequently, RSL3, sorafenib, artemisinin and other molecules were identified for the ability to induce ferroptosis [29,36,37]. In the present work, we found that DSF/Cu, a FDA-approved clinical anti-alcoholism drug, selectively attenuates the abilities of proliferation, migration, invasion and angiogenesis in HCC cells at a low concentration. As mitochondrial dysfunction plays a regulatory role in predicting ferroptotic cell death, further experiments have discovered that DSF/Cu destroys mitochondrial morphology, impairs energy metabolism, accelerates the generation of large quantities of ROS and induces DNA double-strand breaks. Moreover, a range of pharmacological inhibitors of specific cell death pathways was utilized to characterize the basis of cell death induced by DSF/Cu. Both ferroptosis inhibitor and iron chelator were capable of alleviating the cell death initiated by DSF/Cu incubation. Importantly, ferroptotic events, such as catastrophic accumulation of free iron and unrestricted lipid peroxidation, were dramatically accelerated by the treatment of DSF/Cu, and could be significantly blocked by iron chelator DFO. Collectively, the present work provides evidence that DSF/Cu might represent a promising therapeutic agent to preferentially target HCC cells through ferroptosis.

To protect against vulnerability, cancer cells can exploit their defensive mechanisms. NRF2 is a major transcription factor responsible for the regulation of antioxidant response, and plays a critical role in mitigating ferroptosis. Recently, La Rosa et al. have discovered that induction of NRF2 could prevent ferroptosis in FRDA [38]. Increasing evidence has also shown that NRF2 can improve the resistance of cancer cells to chemotherapeutic drugs [7,24]. In HCC, it's confirmed that NRF2 is upregulated in tumor tissues, and transcriptionally activates the ferroptosis-related genes such as HO-1, FTH1, and NQO1, which is associated with malignancy and a poor prognosis [7,39,40]. Therefore, inhibition of Keap1-NRF2-ARE signal system may represent an attractive approach for the reversal of drug resistance. In the resting status of cells, the maintenance of low levels NRF2 depends on the rapid degradation by proteasomes which is mediated by Keap1. Upon oxidative stress, NRF2 gets away from Keap1, translocates into the nucleus and
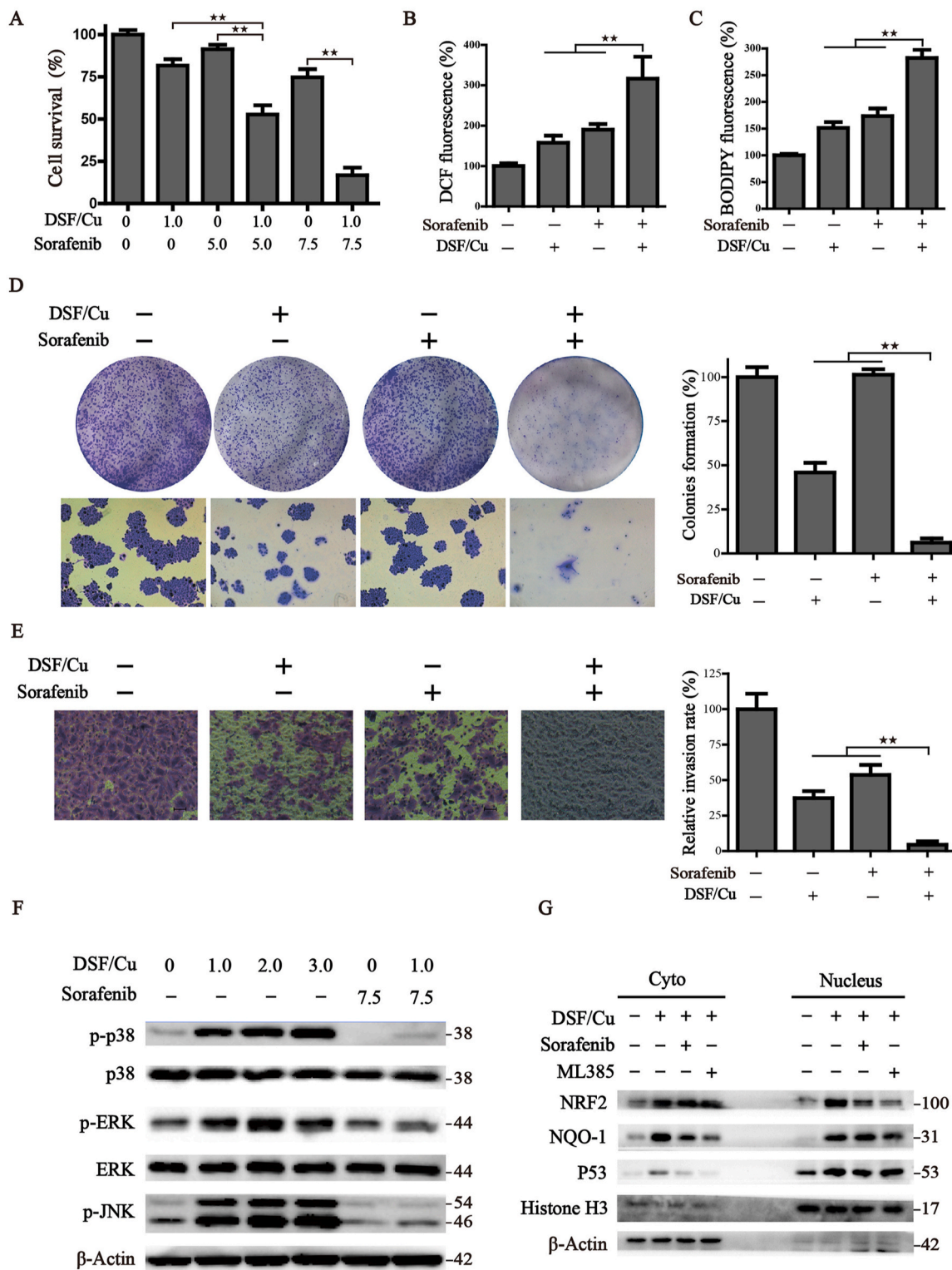
Fig. 6. DSF/Cu acts synergistically with sorafenib against HCC tumors through induction of ferroptosis.
(A) Cells were treated with indicated concentration of DSF/Cu and sorafenib for 12
h, cell survival was detected by CCK8 assay. (B, C) Huh7 cells were treated by mono or combination of DSF/Cu (1.0 μM) and sorafenib (7.5 μM) for 8 h, cellular superoxide and lipid peroxides were measured by DCF-DA and BODIPY staining. (D) The colony-formation assay was performed under the treatment of DSF/Cu (0.1 μM) and/or sorafenib (1.0 μM) for 7 days. The statistical histograms were shown on the right. (E) Transwell assay was conducted to detect the invasion ability of cells under the exposure of DSF/Cu (0.5 μM) and/or sorafenib (7.5 μM), the statistical histograms were shown on the right. (F) The protein expression of Huh7 cells with indicated treatments was detected by Western blot. (G) Cells were treated with DSF/Cu (1.0 μM) alone or in combination with sorafenib (7.5 μM) or ML385 (2.5 μM) for 12 h. The cytoplasmic and nuclear fractions of cells were isolated and subjected to Western blot assay. β-actin and Histone H3 were used as loading controls for the cytosolic and nuclear fractions, respectively. All histograms were presented as mean ± SD. $^{\star}P < 0.05$, $^{\star\star}P < 0.01$ between indicated groups.
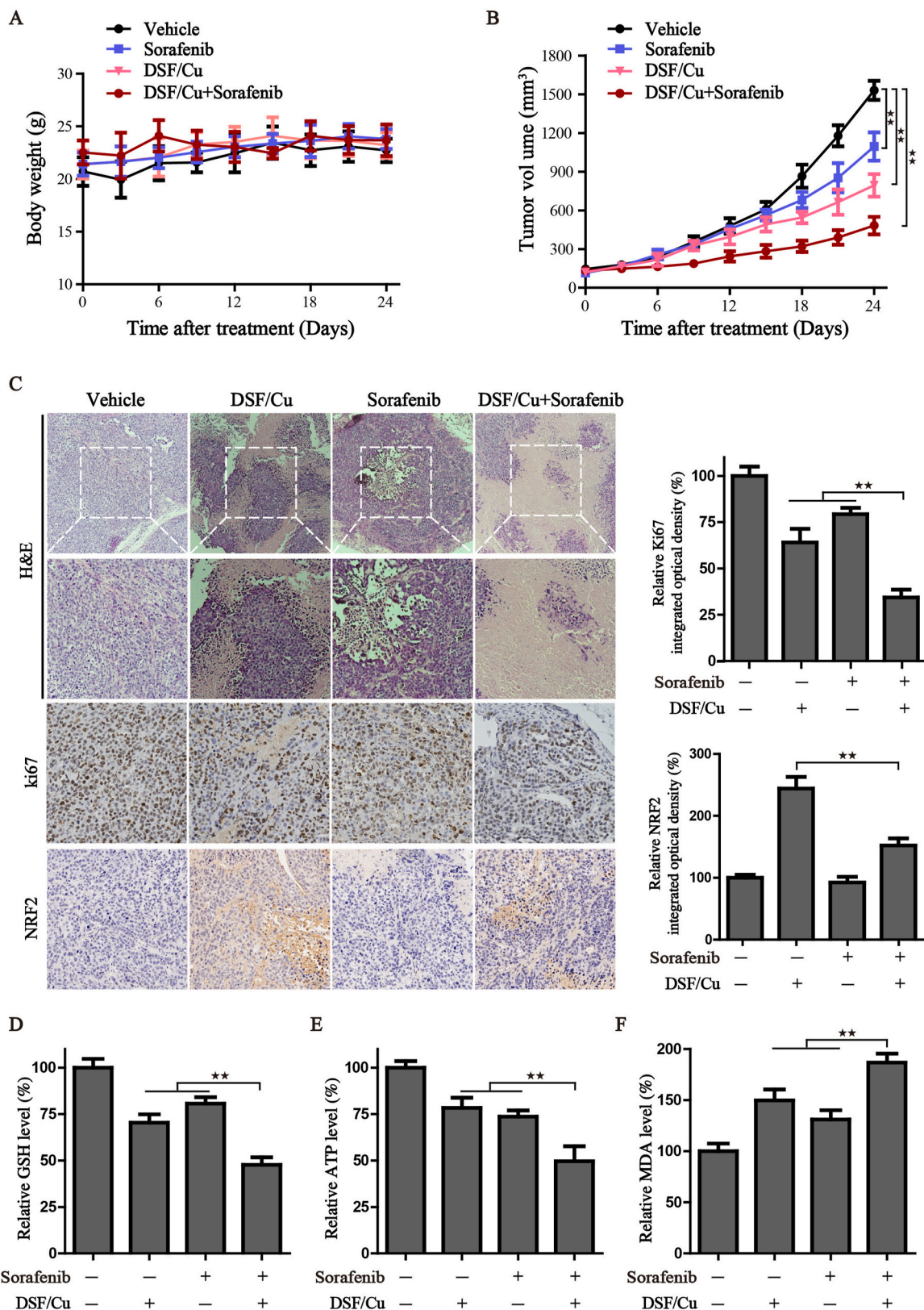
Fig. 7. Combination treatment of DSF/Cu and Sorafenib effectively arrests tumor growth *in vivo*.
Xenografts were established in mice and treated with mono or combination treatment of DSF/Cu and Sorafenib respectively. The body weight (A) and tumor volume (B) were measured every 3 days. (C) H&E staining and IHC analysis for Ki67 and NRF2 in indicated tumor specimens. The statistical expression of Ki67 and NRF2 was shown on the right. (D–
F) The relative GSH, ATP and MDA levels of indicated groups of tumor tissues were measured by commercial kits, respectively. All histograms were represented as mean ± SD. $\star P < 0.05$, $\star\star P < 0.01$ between indicated groups.

binds to the antioxidant element (ARE) located in the upstream promoter region of multiple genes. Therefore, we addressed the question whether the inhibition of NRF2 could act synergistically with DSF/Cu. Our current study revealed that the compensatory activation of the p62-Keap1-NRF2 antioxidative signaling pathway takes part in the protection of DSF/Cu-induced ferroptosis. Either pharmacological or genetic inhibition of the compensatory increased NRF2 expression could strengthen the lipid peroxidation, and sensitize DSF/Cu-induced cell death in HCC cells. Conversely, fostered NRF2 expression was capable of ameliorating the cell death activated by DSF/Cu. Mechanically we found that DSF/Cu dramatically activates the phosphorylation of p62, which facilitates competitive binding to Keap1 for its degradation, thus prolonging the half-life of NRF2. Thus, discovering the defensive mechanism in DSF/Cu-induced cell death is particularly important, which may provide a promising synergistic strategy to overcome drug resistance, and enhance antitumor therapy through ferroptosis.

To date, several NRF2 inhibitors have been screened, including ML385 [25], trigonelline, ATRA, leutolin, and brusatol [41]. Trigonelline, a plant alkaloid, is isolated from the seeds of coffee and fenugreek [42]. For the pharmacological value and low toxicity, trigonelline has been discovered to play a protective role against diabetes. Besides, several beneficial effects of trigonelline have been identified in diseases treatment, such as hyperlipidemia, hyperglycemia and insulin resistance. In the present study, co-incubation of DSF/Cu with trigonelline or ML385 significantly facilitated the accumulation of ROS, and led to a remarkable synergistic inhibitory effect in HCC cells. Moreover, the synergistic antitumor effect of ferroptosis inducers with sorafenib was previously identified in HCC cells [29,43], but no data is available for the combination of sorafenib with DSF/Cu. We uncovered that combination treatment of DSF/Cu and sorafenib effectively arrests HCC cell growth both *in vitro* and *in vivo*. Mechanically, sorafenib attenuated the nuclear translocation of NRF2, and hindered the constant activation of NRF2-ARE pathway in HCC cells. Additionally, simultaneously inhibiting the MAPK kinase signaling pathway is also responsible for the synergistic lethal effects of sorafenib and DSF/Cu.

In summary, DSF/Cu in combination with NRF2 inhibition may provide a promising synergistic strategy to overcome drug resistance and enhance tumor therapy, as it targets ferroptotic cell death and inhibits the protective anti-oxidative stress response in HCC cells. We also provide a framework for further understanding and targeting ferroptosis in cancer therapy.

Declaration of competing interest

The authors declare that there is no conflict of interest.

Fundings and Acknowledgments

List of abbreviations

DCF-DA	2,7-dichlorofluorescin diacetate
DMSO	Dimethyl sulfoxide
ERK	Extracellular signal-regulated kinase
H_2O_2	Hydrogen peroxide
HCC	Hepatocellular carcinoma
JNK	C-Jun NH2-terminal kinase
MAPK	Mitogen-activated protein kinase
NRF2	Nuclear factor erythroid 2-related factor 2
ARE	Antioxidant element
Keap1	Kelch-like ECH-associated protein 1
DSF	Disulfiram
ROS	Reactive oxygen species
NF-κB	Nuclear factor kappa-B
GSH	Glutathione
ATP	Adenosine triphosphate
MDA	Malondialdehyde
Fer-1	Ferrostatin-1
Necro	Necrosuifonamide
NAC	N-acetylcysteine
DFO	Deferoxamine
PI	Propidium iodide
EMT	Epithelial-mesenchymal transition
OCR	Oxygen consumption rate

Appendix A. Supplementary data

Supplementary data to this article can be found online at https://doi.org/10.1016/j.redox.2021.102122.

Ethics approval and consent to participate

Animal experiments were performed in strict adherence with the relevant guidelines and regulations of the Animal Care and Use Committee of the Zhejiang Provincial People's Hospital and approved by the animal ethics committee of the Zhejiang Provincial People's Hospital.

References

[1] H. Sung, J. Ferlay, R. Siegel, M. Laversanne, I. Soerjomataram, A. Jemal, et al., Global cancer statistics 2020: GLOBOCAN estimates of incidence and mortality worldwide for 36 cancers in 185 countries, CA A Cancer J. Clin. 71 (3) (2021) 209–249.

[2] H. El-Serag, Hepatocellular carcinoma, N. Engl. J. Med. 365 (12) (2011) 1118–1127.

[3] R. Siegel, K. Miller, A. Jemal, Cancer statistics, CA A Cancer J. Clin. 68 (1) (2018) 7–30, 2018.

[4] D. Manz, N. Blanchette, B. Paul, F. Torti, S. Torti, Iron and cancer: recent insights, Ann. N. Y. Acad. Sci. 1368 (1) (2016) 149–161.

[5] T. Hirschhorn, B.R. Stockwell, The development of the concept of ferroptosis, Free Radical Biol. Med. 133 (2019) 130–143.

[6] S.J. Dixon, K.M. Lemberg, M.R. Lamprecht, R. Skouta, E.M. Zaitsev, C.E. Gleason, et al., Ferroptosis: an iron-dependent form of nonapoptotic cell death, Cell 149 (5) (2012) 1060–1072.

[7] X. Sun, Z. Ou, R. Chen, X. Niu, D. Chen, R. Kang, et al., Activation of the p62-Keap1-NRF2 pathway protects against ferroptosis in hepatocellular carcinoma cells, Hepatology 63 (1) (2016) 173–184.

[8] S. Zhu, Q. Zhang, X. Sun, H.J. Zeh, M.T. Lotze, R. Kang, et al., HSPA5 regulates ferroptotic cell death in cancer cells, Canc. Res. 77 (8) (2017) 2064–2077.

[9] I. Poursaitidis, X. Wang, T. Crighton, C. Labuschagne, D. Mason, S.L. Cramer, et al., Oncogene-selective sensitivity to synchronous cell death following modulation of the amino acid nutrient cystine, Cell Rep. 18 (11) (2017) 2547–2556.

[10] S. Doll, B. Proneth, Y.Y. Tyurina, E. Panzilius, S. Kobayashi, I. Ingold, et al., ACSL4 dictates ferroptosis sensitivity by shaping cellular lipid composition, Nat. Chem. Biol. 13 (1) (2017) 91–98.

[11] J. Llovet, S. Ricci, V. Mazzaferro, P. Hilgard, E. Gane, J. Blanc, et al., Sorafenib in advanced hepatocellular carcinoma, N. Engl. J. Med. 359 (4) (2008) 378–390.

[12] B. Zhai, X. Sun, Mechanisms of resistance to sorafenib and the corresponding strategies in hepatocellular carcinoma, World J. Hepatol. 5 (7) (2013) 345–352.

[13] M. Frantzi, A. Latosinska, A. Mokou, H. Mischak, A. Vlahou, Drug repurposing in oncology, Lancet Oncol. 21 (12) (2020) e543.

[14] D. Chen, Q. Cui, H. Yang, Q. Dou, Disulfiram, a clinically used anti-alcoholism drug and copper-binding agent, induces apoptotic cell death in breast cancer cultures and xenografts via inhibition of the proteasome activity, Canc. Res. 66 (21) (2006) 10425–10433.

[15] B.W. Morrison, N.A. Doudican, K.R. Patel, S.J. Orlow, Disulfiram induces copper-dependent stimulation of reactive oxygen species and activation of the extrinsic apoptotic pathway in melanoma, Melanoma Res. 20 (1) (2010) 11.

[16] C. Qiu, X. Zhang, B. Huang, S. Wang, W. Zhou, C. Li, et al., Disulfiram, a ferroptosis inducer, triggers lysosomal membrane permeabilization by up-regulating ROS in glioblastoma, OncoTargets Ther. 13 (2020) 10631–10640.

[17] J. Lin, M. Haffner, Y. Zhang, B. Lee, W. Brennen, J. Britton, et al., Disulfiram is a DNA demethylating agent and inhibits prostate cancer cell growth, Prostate 71 (4) (2011) 333–343.

[18] H. Zhang, D. Chen, J. Ringler, W. Chen, Q. Cui, S. Ethier, et al., Disulfiram treatment facilitates phosphoinositide 3-kinase inhibition in human breast cancer cells in vitro and in vivo, Canc. Res. 70 (10) (2010) 3996–4004.

[19] Z. Skrott, M. Mistrik, K.K. Andersen, S. Friis, D. Majera, J. Gursky, et al., Alcohol-abuse drug disulfiram targets cancer via p97 segregase adaptor NPL4, Nature 552 (7684) (2017) 194–199.

[20] Y. Li, L. Wang, H. Zhang, Y. Wang, S. Liu, W. Zhou, et al., Disulfiram combined with copper inhibits metastasis and epithelial-mesenchymal transition in hepatocellular carcinoma through the NF-κB and TGF-β pathways, J. Cell Mol. Med. 22 (1) (2018) 439–451.

[21] T. Chiba, E. Suzuki, K. Yuki, Y. Zen, M. Oshima, S. Miyagi, et al., Disulfiram eradicates tumor-initiating hepatocellular carcinoma cells in ROS-p38 MAPK pathway-dependent and -independent manners, PloS One 9 (1) (2014), e84807.

[22] M. Picard, B. McEwen, E. Epel, Sandi CJFin, An energetic view of stress, Focus on mitochondria 49 (2018) 72–85.

[23] Y. Li, F. Chen, J. Chen, S. Chan, Y. He, W. Liu, et al., Disulfiram/copper induces antitumor activity against both nasopharyngeal cancer cells and cancer-associated fibroblasts through ROS/MAPK and ferroptosis pathways, Cancers 12 (1) (2020) 138.

[24] X. Sun, X. Niu, R. Chen, W. He, D. Chen, R. Kang, et al., Metallothionein-1G facilitates sorafenib resistance through inhibition of ferroptosis, Hepatology 64 (2) (2016) 488–500.

[25] S. Bader, J. Wilmers, M. Pelzer, V. Jendrossek, J. Rudner, Activation of anti-oxidant Keap1/Nrf2 pathway modulates efficacy of dihydroartemisinin-based monotherapy and combinatory therapy with ionizing radiation, Free Radical Biol. Med. 168 (2021) 44–54.

[26] D. Zhang, S. Lo, J. Cross, D. Templeton, M. Hannink, Keap1 is a redox-regulated substrate adaptor protein for a Cul3-dependent ubiquitin ligase complex, Mol. Cell Biol. 24 (24) (2004) 10941–10953.

[27] K. Itoh, N. Wakabayashi, Y. Katoh, T. Ishii, K. Igarashi, J. Engel, et al., Keap1 represses nuclear activation of antioxidant responsive elements by Nrf2 through binding to the amino-terminal Neh2 domain, Gene Dev. 13 (1) (1999) 76–86.

[28] Y. Ichimura, S. Waguri, Y-s Sou, S. Kageyama, J. Hasegawa, R. Ishimura, et al., Phosphorylation of p62 activates the keap1-nrf2 pathway during selective autophagy, Mol. Cell. 51 (5) (2013) 618–631.

[29] Y. Li, J. Xia, F. Shao, Y. Zhou, J. Yu, H. Wu, et al., Sorafenib induces mitochondrial dysfunction and exhibits synergistic effect with cysteine depletion by promoting HCC cells ferroptosis, Biochem. Biophys. Res. Commun. 534 (2021) 877–884.

[30] J. Yuan, X. Dong, J. Yap, J. Hu, The MAPK and AMPK signalings: interplay and implication in targeted cancer therapy, J. Hematol. Oncol. 13 (1) (2020) 113.

[31] B.A. Carneiro, W.S. El-Deiry, Targeting apoptosis in cancer therapy, Nat. Rev. Clin. Oncol. 17 (Suppl. 13) (2020).

[32] J. Du, Y. Zhou, Y. Li, J. Xia, Y. Chen, S. Chen, et al., Identification of Frataxin as a regulator of ferroptosis, Redox Biol 32 (2020) 101483.

[33] K. Bersuker, J.M. Hendricks, Z. Li, L. Magtanong, B. Ford, P.H. Tang, et al., The CoQ oxidoreductase FSP1 acts parallel to GPX4 to inhibit ferroptosis, Nature 575 (7784) (2019) 688–692.

[34] M. Gao, J. Yi, J. Zhu, A.M. Minikes, P. Monian, C.B. Thompson, et al., Role of mitochondria in ferroptosis, Mol. Cell. 73 (2) (2019) 354–363 e353.

[35] I. Ingold, C. Berndt, S. Schmitt, S. Doll, G. Poschmann, K. Buday, et al., Selenium utilization by GPX4 is required to prevent hydroperoxide-induced ferroptosis, Cell 172 (3) (2018) 409–422 e421.

[36] J. Du, T. Wang, Y. Li, Y. Zhou, X. Wang, X. Yu, et al., DHA inhibits proliferation and induces ferroptosis of leukemia cells through autophagy dependent degradation of ferritin, Free Radical Biol. Med. 131 (2018) 356–369, https://doi.org/10.1016/j.freeradbiomed.2018.12.011.

[37] J. Du, X. Wang, Y. Li, X. Ren, Y. Zhou, W. Hu, et al., DHA exhibits synergistic therapeutic efficacy with cisplatin to induce ferroptosis in pancreatic ductal adenocarcinoma via modulation of iron metabolism, Cell Death Dis. 12 (7) (2021) 705.

[38] P. La Rosa, S. Petrillo, R. Turchi, F. Berardinelli, T. Schirinzi, G. Vasco, et al., The Nrf2 induction prevents ferroptosis in Friedreich's Ataxia, Redox biology 38 (2020) 101791.

[39] Q. Wang, C. Bin, Q. Xue, Q. Gao, A. Huang, K. Wang, et al., GSTZ1 sensitizes hepatocellular carcinoma cells to sorafenib-induced ferroptosis via inhibition of NRF2/GPX4 axis, Cell Death Dis. 12 (5) (2021) 426.

[40] M.J. Kerins, A. Ooi, The roles of NRF2 in modulating cellular iron homeostasis, Antioxidants Redox Signal. 29 (17) (2018) 1756–1773.

[41] Y. Murakami, K. Sugiyama, H. Ebinuma, N. Nakamoto, K. Ojiro, P. Chu, et al., Dual effects of the Nrf2 inhibitor for inhibition of hepatitis C virus and hepatic cancer cells, BMC Canc. 18 (1) (2018) 680.

[42] J. Zhou, L. Chan, S. Zhou, Trigonelline: a plant alkaloid with therapeutic potential for diabetes and central nervous system disease, Curr. Med. Chem. 19 (21) (2012) 3523–3531.

[43] Z. Li, H. Dai, X. Huang, J. Feng, J. Deng, Z. Wang, et al., Artesunate synergizes with sorafenib to induce ferroptosis in hepatocellular carcinoma, Acta Pharmacol. Sin. 42 (2) (2021) 301–310.